scientific reports

Check for updates

OPEN

Oncolytic alphavirus-induced extracellular vesicles counteract the immunosuppressive effect of melanoma-derived extracellular vesicles

Darshak K. Bhatt[1,2], Annemarie Boerma[1], Silvina Odete Bustos[2,3], Andréia Hanada Otake[2,3], Alexis Germán Murillo Carrasco[2,3], Patrícia Pintor Reis[4], Roger Chammas[2,3,5]✉, Toos Daemen[1,5] & Luciana Nogueira de Sousa Andrade[2,3,5]✉

Extracellular vesicles (EVs)-mediated communication by cancer cells contributes towards the pro-tumoral reprogramming of the tumor microenvironment. Viral infection has been observed to alter the biogenesis and cargo of EVs secreted from host cells in the context of infectious biology. However, the impact of oncolytic viruses on the cargo and function of EVs released by cancer cells remains unknown. Here we show that upon oncolytic virotherapy with Semliki Forest virus-based replicon particles (rSFV), metastatic melanoma cells release EVs with a distinct biochemical profile and do not lead to suppression of immune cells. Specifically, we demonstrate that viral infection causes a differential loading of regulatory microRNAs (miRNAs) in EVs in addition to changes in their physical features. EVs derived from cancer cells potentially suppress splenocyte proliferation and induce regulatory macrophages. In contrast, EVs obtained from rSFV-infected cells did not exhibit such effects. Our results thus show that rSFV infection induces changes in the immunomodulatory properties of melanoma EVs, which may contribute to enhancing the therapeutic efficacy of virotherapy. Finally, our results show that the use of an oncolytic virus capable of a single-round of infection allows the analysis of EVs secreted from infected cells while preventing interference from extracellular virus particles.

Keywords Extracellular vesicles, Oncolytic virus, Immunomodulatory, Melanoma

Tumor-derived extracellular vesicles (EVs) have been identified as key players in the regulation of tumor-immune interactions and cancer progression. EVs are produced by all cell types and are known to originate from endosomes and/or the cellular plasma membrane[1]. These vesicles serve as vehicles for transporting bioactive materials, such as proteins, lipids, and genetic material, to recipient cells, influencing various aspects of their function and response[1,2]. This has important implications for oncolytic viruses used in cancer treatment as viral infection may impact cellular communication by regulating the biogenesis and cargo of tumor-derived EVs[3–5]. Virotherapy-induced changes in EV composition may result in phenotype regulation of recipient immune cells, ultimately affecting therapeutic outcomes. Therefore, understanding the extent to which oncolytic viruses influence the characteristics of EVs remains a crucial area of research.

Previous reports have investigated several aspects related to the interaction between EVs and viruses. These studies have explored strategies of viruses encapsulating within EVs to improve delivery and evade antiviral antibodies[6,7], how EVs allow capsid-independent transfer of viral genomes between cells[8,9], the differential

[1]Department of Medical Microbiology and Infection Prevention, University Medical Center Groningen, University of Groningen, Groningen 9713 AV, The Netherlands. [2]Center for Translational Research in Oncology (LIM/24), Instituto do Cancer do Estado de Sao Paulo, Hospital das Clinicas HCFMUSP, Faculdade de Medicina, Universidade de Sao Paulo, São Paulo CEP 01246-000, Brazil. [3]Comprehensive Center for Precision Oncology (C2PO), Universidade de Sao Paulo, São Paulo, Brazil. [4]Department of Surgery and Orthopedics and Experimental Research Unity (UNIPEX), Faculdade de Medicina, Universidade Estadual Paulista (UNESP), Botucatu 18618-687, Brazil. [5]These authors jointly supervised this work: Roger Chammas, Toos Daemen and Luciana Nogueira de Sousa Andrade. ✉email: rchammas@usp.br; luciana.nsandrade@hc.fm.usp.br

sorting of microRNAs (miRNAs) in EVs from infected cells[10], and the possibility of exploiting EV-mediated communication to induce systemic immunity[11] or sensitize cancer cells to virotherapy[10,12]. However, it has been noted that evaluation of EVs secreted from virus-infected cells is challenging due to the similarities in size and biochemical features between viruses and vesicles[13,14], such as the presence of a lipid layer envelope containing cellular membrane proteins, as well as their use of similar secretory pathways for extracellular release and fusion with recipient cells[13]. Furthermore, the presence of oncolytic virus within EVs has been found to induce immune-independent abscopal effects by directly mediating cytotoxic activity to distal tumors[15]. This emphasizes the need for careful isolation and characterization of EVs from virus-infected cells while avoiding the presence of extracellular virus particles.

In order to prevent the infected cells from producing new virus particles, we employed the use of recombinant oncolytic Semliki Forest virus capable of a single round of infection. Semliki Forest virus (SFV) is a positive-stranded RNA virus. The RNA genome of SFV is a replicon, meaning self-replicating, as it encodes non-structural proteins responsible for RNA replication and translation. Recombinant SFV (rSFV) replicon particles can be produced through the use of a two-helper RNA system where the genes encoding viral structural proteins are expressed from an independent RNA molecule devoid of a viral-packaging signal, thus ensuring that the infected cells do not continue to produce viruses[16–18]. This allows for the isolation and characterization of tumor EVs without extracellular virus-contamination. The potential of rSFV as an oncolytic and immunogenic virus has been evaluated extensively in murine models. In addition, we have recently shown that rSFV can be engineered to express human cytokines or chemokines, effectively recruiting and activating T cells in human cancer models. Additionally, our group demonstrated phase-1 clinical safety and immunogenic potential of an rSFV-based vaccine encoding human papillomavirus antigens in cervical cancer patients[19].

Tumor EVs play an active role in the dynamic and complex tumor-immune signaling that occurs in the tumor microenvironment. Similar to various other cancer types, EVs from melanoma have been found to promote cancer survival through pro-tumoral and immunoregulatory mechanisms[2,20,21]. Multiple studies have shown that melanoma EVs, especially exosomes (or small vesicles, 30–150 nm sized EVs) of the B16F10 model, can promote tumor progression and immune evasion through transfer of survival-promoting signals[22] presence of immunoregulatory signals[23,24], and neutralization of checkpoint inhibitors[25]. Therefore, we used the B16F10 model to study changes in the functional profile of melanoma EVs by rSFV-replicon particles. We systematically investigated the ability of EVs secreted from rSFV-infected cancer cells to regulate the phenotype of recipient cancer cells and immune cells. Specifically, we first assessed the difference in physical features of EVs from rSFV-infected cells. Next, we studied the survival of cancer cells, activation of lymphocytes, and phenotypic polarization of macrophages in response to EVs from rSFV-infected or non-infected cells. Finally, we identified the differentially enriched miRNA cargo in EVs from rSFV-infected cells which explains, at least in part, the functional differences observed in our experiments.

Results

Isolation and physical characterization of EVs released upon SFV-infection

Replicating wild-type SFV infection has been associated with changes in the expression of genes involved in the regulation of EV synthesis and release (Supplementary Fig. 1), indicating that EVs from healthy albeit infected cells may have a different composition or function as compared to non-infected cells. Therefore, we first set out to isolate and characterize EVs released from melanoma cells post viral infection. We infected B16F10 melanoma cells with a MOI-10 of rSFV encoding GFP (SFV-GFP) (Fig. 1A) and performed a PBS-wash after 2 h of infection to remove extracellular rSFV particles from the supernatant. Upon 24 h post-infection, the supernatant was collected and the EVs were isolated through serial ultracentrifugation (Fig. 1B). Between independent batches of EV preparations, we observed minimal variations in the overall yield of EVs obtained from infected (SFV EVs) and non-infected cells (NT EVs) (Fig. 1C). However, considering the reduction in cell numbers due to oncolysis in the rSFV-infected condition, we noticed a substantial increase in the vesicle-per-cell ratio from infected cells compared to non-infected cells (Fig. 1D, E). B16F10 cells produced a heterogeneous population of EVs with most of the EVs being around 200 nm in diameter, with infected cells notably producing larger-sized EVs as well (> 300 nm diameter) (Fig. 1F). EVs from both infected and non-infected cells showed a strongly negative zeta potential, confirming their stability; however, SFV EVs displayed a significantly more negative zeta potential indicating a slight distinct physicochemical profile (Fig. 2A). Through a western blot assay, we validated the presence of tetraspanins (vesicle membrane-associated proteins) in EV preparations; where EVs from infected cells were enriched in CD63 membrane proteins as compared to CD9 enriched EVs from non-infected cells (Fig. 2B). The presence of multiple CD63 bands is often associated with the existence of isoforms, which can be attributed to variations in its glycosylation status[26]. The CD63 enrichment in SFV EVs paralleled the CD63 upregulation observed in SFV-infected cells (Supplementary Fig. 1). Finally, we performed transmission electron microscopy (TEM) to visualize the ultrastructure of the EV isolates. Particles observed from sample preparations of EVs from non-infected and rSFV-infected cells were observed to have a spherical appearance (Fig. 2C).

Effect of SFV EVs on melanoma cells

Melanoma EVs have the potential to transfer pro-tumoral survival signals to recipient melanoma cells and promote tumor progression[27–29]. Therefore, we tested if rSFV-infection could alter the communication dynamics or the pro-tumoral potential of melanoma EVs. First, we labeled SFV- or NT EVs with a fluorescent lipophilic dye and quantified their uptake by B16F10 melanoma cells over time. Although no disparities were noted after 24 h via fluorescence microscopy (Supplementary Fig. 2A–D), earlier time points (up to 6 h) assessed via flow cytometry, revealed significant differences. Specifically, SFV EVs were assimilated into cells at a faster rate than NT EVs. Notably, after 6 h, the rate of EV uptake plateaued irrespective of EV type. (Supplementary Fig. 2E–G).

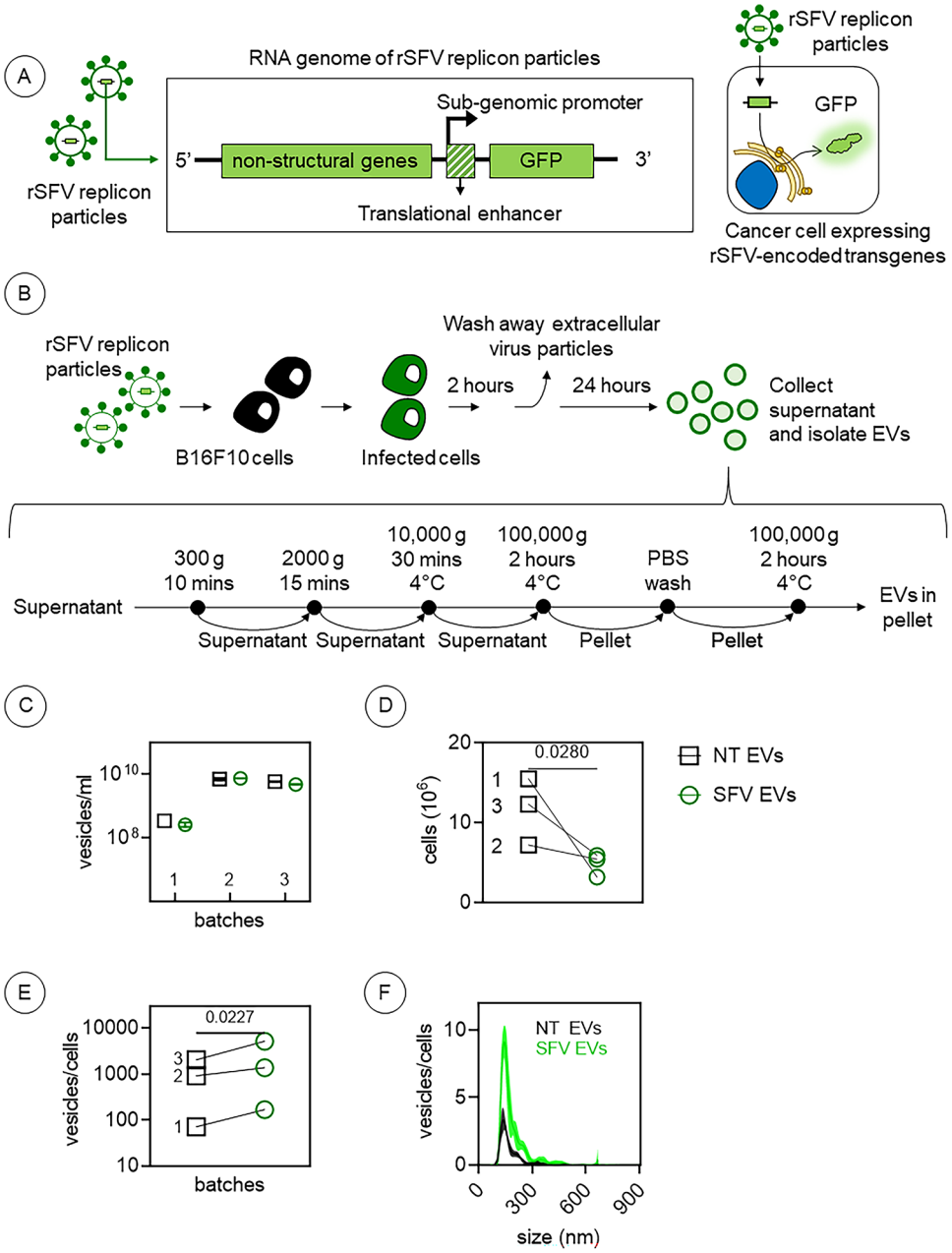

Fig. 1. Isolation of tumor-derived EVs upon exposure to rSFV replicon particles. (**A**) Semliki Forest virus replicon particles were engineered by replacing the structural genes in the genome with a GFP-transgene (left) to enable a single round of infection (right). (**B**) Illustration of the experimental scheme for rSFV infection of B16F10 cells followed by a wash 2 h post-infection to remove extracellular virus particles and incubation for 24 h before the collection of supernatants followed by EV isolation through sequential ultracentrifugation steps. (**C**) Absolute vesicle yield from infected (rSFV EVs) or non-infected B16F10 cells (NT EVs) in different batches. (**D**) Decrease in the number of viable B16F10 cells upon rSFV infection. (**E**) Vesicles per cell count based on number of cells present at the time of EV isolation. (**F**) Size distribution of EVs from infected and non-infected cells. In (**C**–**E**) $n = 3$ independent batches of EV-preparation are shown. Data are presented as mean values. One-way ANOVA followed by Bonferroni's multiple comparisons test was performed.

Moreover, EVs from infected cells did not show cytotoxic effects on the B16F10 cells (Supplementary Fig. 2D). We next evaluated if EVs from infected cells influenced the process of tumor development through an in vivo experiment. We treated B16F10 cells every 24 h with EVs for 5 days and then injected them subcutaneously in C57BL6 mice to study the efficacy of tumor engraftment (Fig. 3A). B16F10 melanoma cells treated with EVs from non-infected cells developed tumors in all mice, in contrast to treatment with EVs from SFV-infected cells, where 40% of the animals did not develop tumors up to 40 days after injection (Fig. 3B), indicating that EVs from infected cells might impair melanoma engraftment. Although we observed a delay in engraftment,

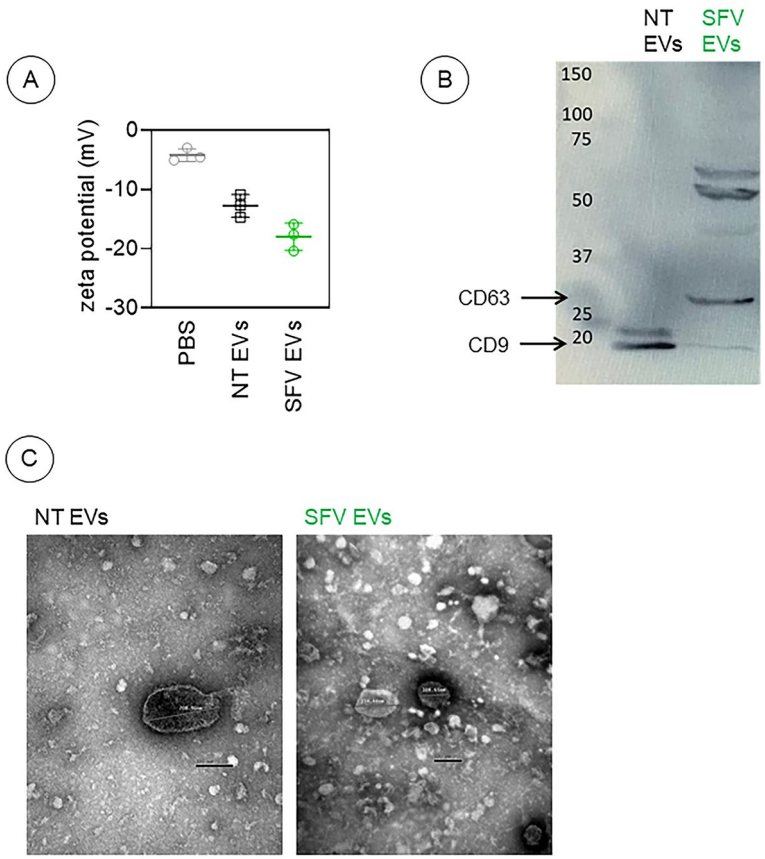

Fig. 2. Characterization of tumor-derived EVs upon exposure to rSFV replicon particles. (**A**) Zeta potential of SFV EVs and NT EVs. (**B**) Western blot image for validation of expression of CD63 and CD9 as EV membrane markers in the EV-preparations. (**C**) Transmission electron microscopy of vesicles from non-infected and SFV-infected melanoma cells. In (A) Data are presented as mean values.

the rate of tumor growth was not significantly different when measured from the point at which tumors became measurable and tracked until they reached or surpassed a size of 1 cubic centimeter. (Fig. 3C).

Then, to investigate if EVs from infected cells negatively influenced the tumorigenic potential of melanoma cells, we performed an in vitro experiment to assess their clonogenic potential. Interestingly, in contrast to the results from the in vivo experiment, EVs from infected cells led to a significant increase of 25% in the number of B16F10 colonies as compared to EVs from non-infected cells (Fig. 3D, E). Simultaneously, we tested if EVs from infected cells could confer resistance to infection in recipient melanoma cells and thereby improve tumor survival (Supplementary Fig. 3A). Pre-treatment of B16F10 melanoma cells with EVs from infected cells did not lead to resistance but rather led to a 5–10% increase in the susceptibility to virus infection as quantified through the number of GFP-positive cells (Supplementary Fig. 3B, C). Of note, GFP expression was not observed in melanoma cells upon treatment with EVs alone. Moreover, pre-treatment with EVs from infected cells also did not alter the susceptibility of cells to rSFV-mediated impairment of tumor clonogenicity (Supplementary Fig. 3D, E).

Then, to elucidate the mechanisms behind the tumor rejection observed in animals injected with SFV EVs-treated cells, we next assessed the changes in gene expression of melanoma cells educated with EVs from non-infected or rSFV-infected cells (Fig. 4A, B). We observed that treatment by EVs from rSFV-infected cells did not lead to expression of SFV-associated viral genes in recipient melanoma cells as expected. On the other hand, the expression profiles of some innate immune genes were found to be altered. Notably, a significant upregulation of *Pd-l1* expression was noted in recipient melanoma cells upon treatment with EVs from non-infected cells (NT EVs) which could be involved in the establishment of an immunosuppressive environment. In addition, to verify whether these EVs could indirectly influence the cytotoxic activity of T lymphocytes leading to the rejection of tumors in animals injected with SFV EVs-treated cells, we performed a co-culture assay consisting of splenocytes from healthy mice in presence of EV-educated melanoma cells (Fig. 4C, D). EVs from rSFV-infected cells were found to promote cytotoxic CD8 T cell activation (Fig. 4E) but not helper CD4 T cell activation (Fig. 4F), although there was no difference in the frequencies of dead or apoptotic melanoma cells due to either of EV-pretreatment (Fig. 4G). Based on these results, we suggest that the rejection observed in animals injected with SFV EVs-treated cells may be related to the alterations in the tumor microenvironment (TEM) imposed by reprogrammed tumor cells. Although these alterations led to an increase in the frequency of CD8 cells, they

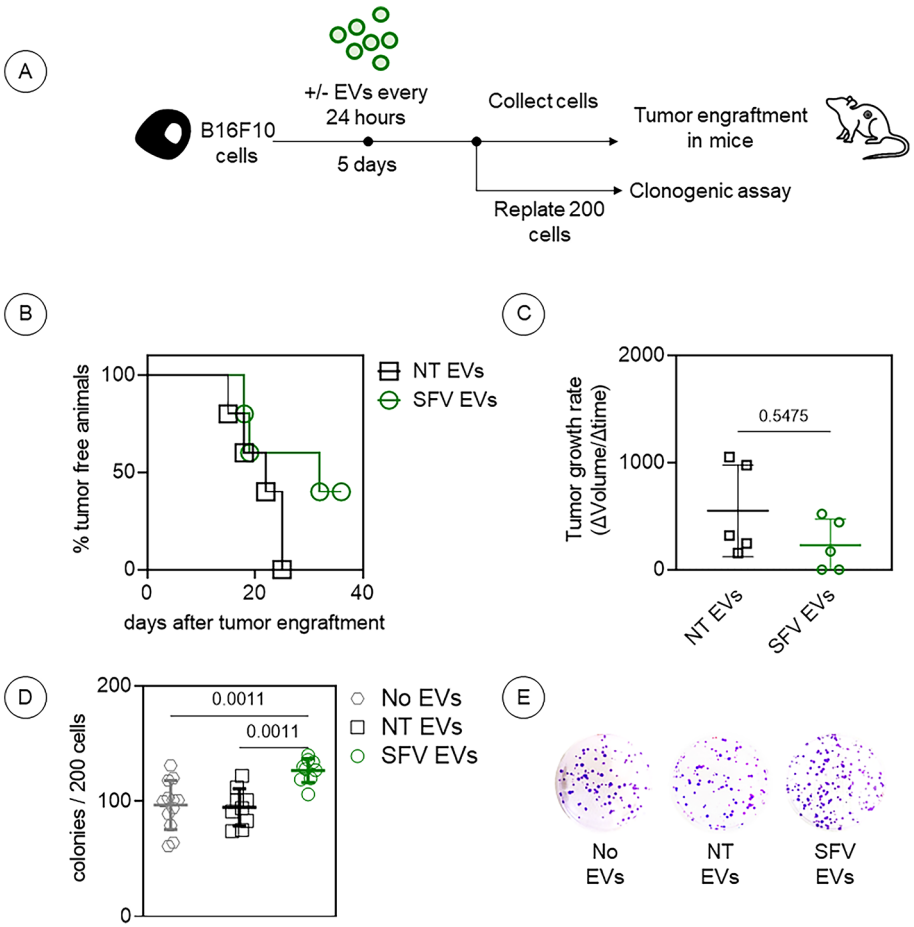

Fig. 3. The effect of rSFV-induced EVs on tumor establishment. (**A**) Overall scheme of the experimental steps where B16F10 cells were pre-treated with EVs from infected (SFV EVs) or non-infected cells (NT EVs) daily for 5 days and then collected for an in vivo tumor engraftment assay or an in vitro clonogenic assay. (**B**) Percentage of animals free from tumor and (**C**) related tumor growth rate upon injection with B16F10 cells pretreated with SFV EVs or NT EVs ($n = 5$ for each group). (**D**) Frequency of colonies formed from 200 cells plated after 7 days of clonogenic assay. (**E**) Representative images of colonies in a well formed by B16F10 cells from different conditions. In (**D**,**E**) $n = 12$ replicates from 4 independent experiments. One-way ANOVA followed by Bonferroni's multiple comparisons test was performed. Data are presented as mean values ± SD.

did not enhance their anti-tumoral activity, which could be attributed to the influence of other immune cells recruited to the TEM.

Effect of SFV EVs on modulating macrophage polarization

Tumor EVs have been described to directly regulate the activity of tumor-associated myeloid cells and to alter their phenotype to a more M2-like wound-healing and regulatory profile, rather than an M1-like inflammatory profile[30–32]. Therefore, we tested if rSFV infection could alter melanoma EVs and regulate the macrophage phenotype to a pro-inflammatory type. For this, bone-marrow-derived murine macrophages were polarized to either an M1-like or M2-like phenotype through cytokine stimulation in the presence of EVs from infected or non-infected cells (Fig. 5A). In macrophages initially polarized towards an M2-like phenotype, we observed that EVs from melanoma cells further promoted the regulatory phenotype through upregulation of *Mrc-1* (CD206) and arginase (*Arg-1*) gene expression and an observable but statistically insignificant downregulation of *Il12* and *iNOS* expression (Fig. 5B–E). In contrast, EVs from infected cells demonstrated more pro-inflammatory effects by inhibiting the upregulation of *Mrc-1* and arginase expression and a trend towards promoting *Il12* and *iNOS* expression. Alternatively, in naive M0-like or M1-like macrophages EVs from melanoma cells upregulated the expression of *iNOS*, indicating a context-dependent or mixed functional profile (Fig. 5E). No differences were observed among groups concerning *Il10* (Fig. 5F).

Effect of SFV EVs on the activation of splenocytes

In addition to myeloid cells, melanoma EVs have also been reported to regulate activation and regulation of lymphocyte function in tumors[25,33]. So, we hypothesized that changes in melanoma EVs induced by rSFV infection may also influence the regulation of lymphocyte activation. We studied lymphocyte activation through

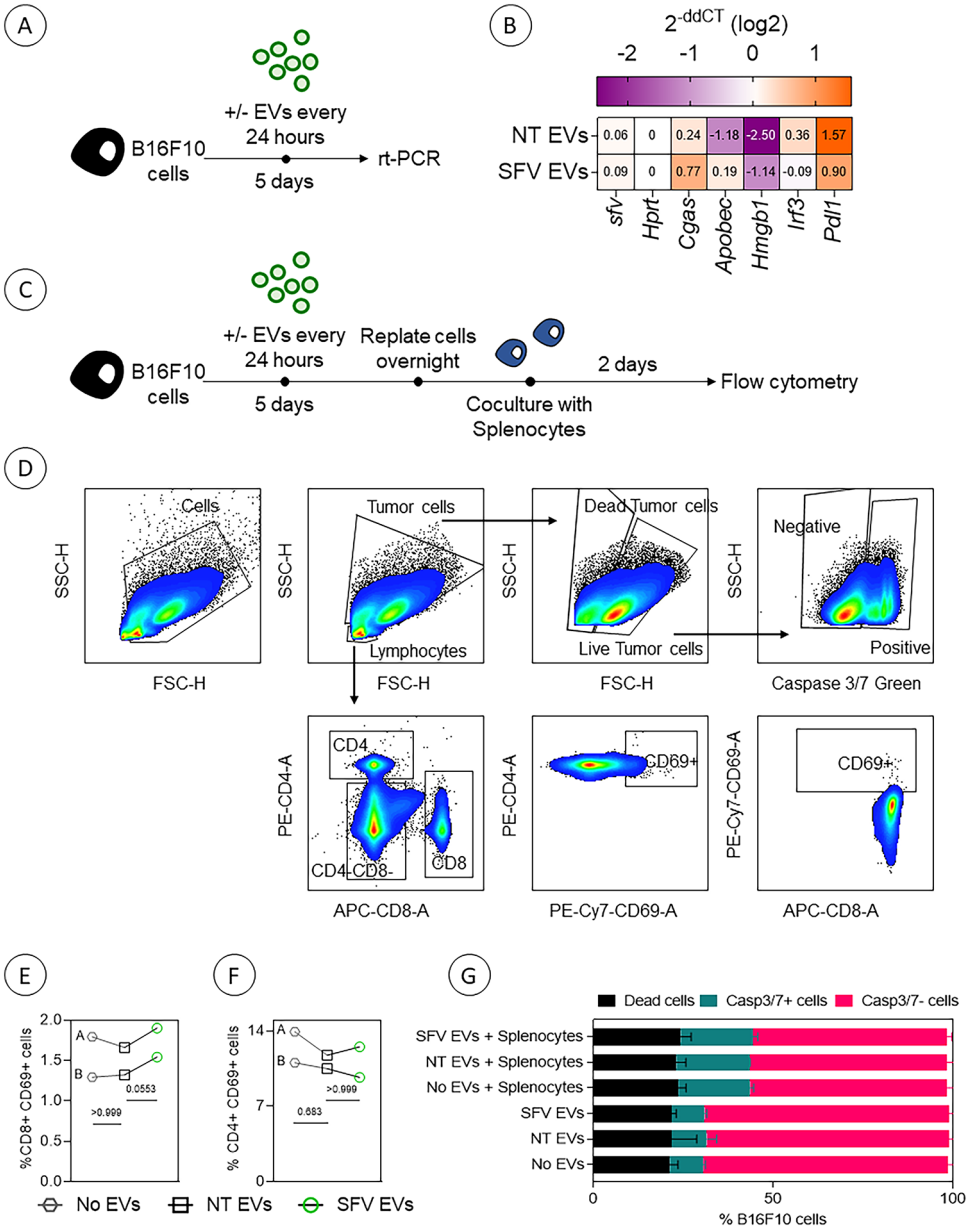

Fig. 4. Immunoregulatory phenotype of melanoma cells upon exposure to EVs from rSFV-infected or non-infected cells. (**A**) Experimental scheme to study changes in gene expression of melanoma cells upon vesicle treatment. (**B**) Heatmap of gene expression upon treatment with vesicles from non-infected or SFV-infected melanoma cells. (**C**) Experimental setup of co-culture of vesicle treated melanoma cells and splenocytes. (**D**) Flow cytometry analysis of tumor cell-death and CD4 and CD8 T cell activation. Frequency of active (**E**) cytotoxic CD8 T cells or (**F**) helper CD4 T cells expressing CD69. (**G**) Frequency of melanoma cells that are dead, apoptotic (Casp3/7+) or non-apoptotic (Casp3/7-). In (**A**) $n=4$ replicates. In (**B**) $2^{-\Delta\Delta Ct}$ values were calculated with respect to endogeneous (*Hprt*) gene expression and plotted as fold change data points on a log2 axis for 3 replicates. Cells not treated with EVs (No EVs group) was used as reference sample. In (**C**) the replicates represent data from 2 splenocytes isolated from healthy mice. In E, F and G, the labels A and B represent data from the two different splenocytes.

mitogenic stimulation of splenocytes and measured splenocyte proliferation in the presence of melanoma EVs (Fig. 6A). We observed that melanoma EVs significantly reduced the activation-induced proliferation of splenocytes, whereas the magnitude of inhibition was not as strong in the case with EVs from infected cells (Fig. 6B, C). Through absolute count of splenocytes and CFSE-based analysis of cell proliferation, we confirmed that melanoma EVs slowed down the proliferative potential of splenocytes.

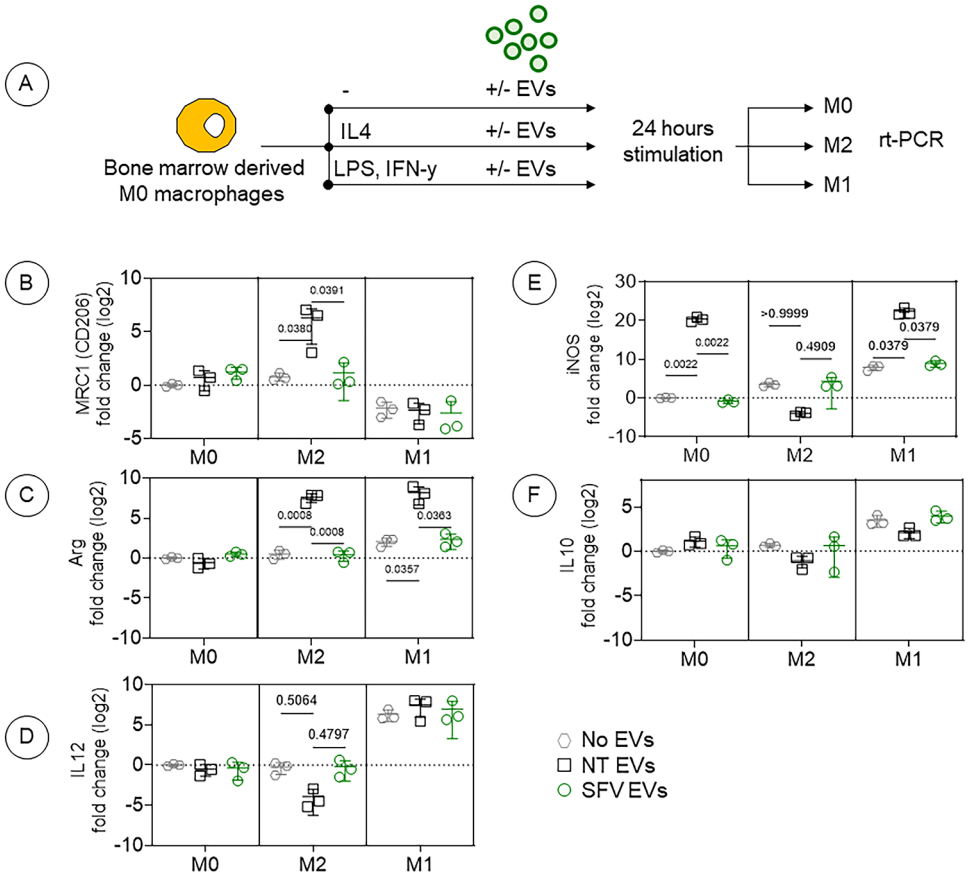

Fig. 5. The effect of rSFV-induced EVs on macrophage polarization. (**A**) Illustration of the experiment where bone-marrow derived macrophages were polarized to inflammatory M1-like or regulatory M2-like macrophages in presence of EVs from infected (SFV EVs) or non-infected cells (NT EVs). Polarization towards an M1-like phenotype was done through treatment with LPS and IFN-y, while towards an M2-like phenotype was done with IL-4. Macrophage polarization was assessed by quantification of mRNA expression of (**B**) *Mrc1*, (**C**) *Arg1*, (**D**) *Il12*, (**E**) *iNos*, and (**F**) *Il10*, with H*prt* used as an endogenous housekeeping gene. In (**B**–**F**) bone-marrow derived macrophages tested from $n = 3$ animals in independent experiments. Data are presented as mean values ± SD.

Differences in the miRNA cargo of SFV EVs

The current literature in the field of EVs has shown that EVs confer changes in functional phenotypes of recipient cells through various biochemical signals in the form of lipids, proteins, and nucleotides, among others[21]. Recently, there has been an increased interest in studying the role of non-coding RNA sequences, mainly miRNAs that are transferred through EVs and have a potent role in gene expression regulation in target cells. Moreover, some studies have shown that transfer of miRNAs from infected cancer cells to other cancer cells can further sensitize the cells for infection and that one can engineer viruses to exploit the EV-mediated delivery of miRNAs[10,12]. Herein, we observed that rSFV infection indeed caused differences in miRNAs packaged in EVs as compared to the ones from uninfected cells (Fig. 7A). Relevantly, eight miRNAs were described as highly expressed in SFV EVs (mmu-miR-1193, mmu-miR-1898, mmu-miR-1963, mmu-miR-568, mmu-miR-652, and mmu-miR-669a). On the other hand, miRNAs from the let-7 family achieved higher levels in NT EVs. Among the miRNAs overexpressed in SFV EVs, we identified a median of 30 validated gene targets, ranging from 1 for mmu-miR-1963 to 538 for mmu-miR-652-3p. While these results may be influenced by the number of studies available for each miRNA, we observed that the targets of mmu-miR-652-3p are particularly enriched in pathways such as the regulation of small molecule metabolic processes and gene expression activation (Fig. 7B). In addition, targets of this miRNA were found highly expressed in macrophages (Fig. 7C, $p < 0.001$), followed by monocytes, endothelial cells, and fibroblasts. Complementing these observations, targets from mmu-miR-669a were found enriched in T cells ($p < 0.001$), highlighting that the presence of rSFV in melanoma cells affects the sorting of microRNAs into EVs which may impact in their effect on recipient cells especially in macrophages. A complete list of enriched pathways for the targets of this miRNA is provided in Supplementary Table S1.

Discussion

Our study investigated the effect of rSFV on the characteristics and functionality of EVs released by rSFV-infected melanoma cells. Our results demonstrate that infection with rSFV induced changes in the physicochemical

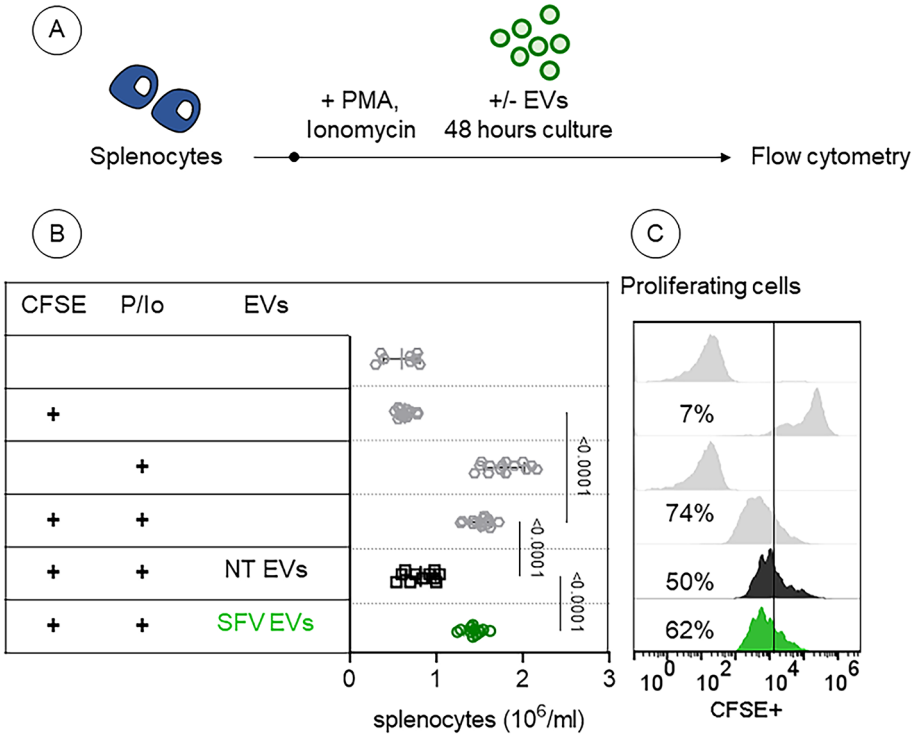

Fig. 6. The effect of rSFV-induced EVs on splenocyte activation and proliferation. (**A**) Illustration of the experimental steps where freshly isolated splenocytes from mice were labeled with CFSE and then activated with PMA and ionomycin in the presence of EVs from infected (SFV EVs) or non-infected cells (NT EVs). 48 h post treatment, CFSE-labeled splenocytes were (**B**) counted manually and (**C**) analyzed by flow cytometry to observe CFSE-based proliferation profiles. Splenocytes were isolated from $n = 4$ animals for independent experiments. Data are presented as mean values ± SD.

properties of EVs. This included an increase in their concentration and size, along with alterations in miRNA cargo. Notably, the sorting of miRNAs in EVs from rSFV-infected cells was found to be different, indicating that virotherapy can influence the packaging of specific miRNAs within EVs. Moreover, we observed that these EVs from rSFV-infected melanoma cells reduced tumor engraftment in mice. This effect could be partially attributed to the reprogramming of tumor cells by EVs characterized by *Pd-l1* upregulation that can be involved in the establishment of an immunosuppressive environment. Our findings shed light on how virotherapy based on rSFV affects the cargo and function of EVs, highlighting their potential role in modulating the immune response and tumor progression.

Based on our findings, EVs from rSFV-infected cells have distinct features compared to EVs from uninfected cells. For instance, EVs from infected cells had a significantly distinct physiochemical profile in terms of size and membrane potential. This may hint towards a difference in the biomolecular composition of EVs or possibly at the differential regulation of EV biogenesis between infected versus non-infected cells[2,5]. Furthermore, distinct physicochemical features of EVs could impact their stability, aggregation, or uptake by recipient cells, ultimately influencing signaling in the tumor microenvironment[34–36]. In the context of biochemical features, EVs from infected cells were enriched in exosomal marker (CD63), while those from uninfected cells were enriched in ectosomal marker (CD9)[37]. Our data also suggest a slight increase (5%) in infectivity by SFV-GFP particles upon preincubation of melanoma cells with EVs from infected cells. This might be partly explained by the fact that CD63 has been found to be involved in several stages of exosomal release and its enrichment in EVs positively correlates with virus infection and spread[38–41]. Moreover, our study found that rSFV infection of melanoma cells impacted the packaging of specific miRNAs in EVs. This is consistent with previous studies that have reported the selective sorting of miRNAs into EVs upon viral infection[10] and also the protein content as recently demonstrated by Hirigoyen[42]. This might suggest miRNA-dependent phenotypic differences in the recipient cells that we observed in our study, where miRNAs may regulate the survival of cancer cells or the activation profile of immune cells[43,44]. Interestingly, concerning the targets of the most abundant microRNAs found in SFV EVs, in particular mmu-miR-652-3p, we noticed that they are highly expressed in macrophages. Indeed, one of the targets of this microRNA is STAT3, a key player in macrophage polarization[45]. Then, based on that, we suggest that the differential EV effect we found between SFV and NT EVs in the macrophage gene expression profile can be a result from the transfer of specific microRNAs by SFV EVs that can modify macrophage phenotype through downregulation of STAT3, for example, promoting the acquisition of M1-like phenotype. Overall, the sorting of specific miRNAs in EVs upon virotherapy may hold clinical significance, offering insights into cancer progression and therapeutic responses. EVs with distinct miRNA profiles may serve as prognostic

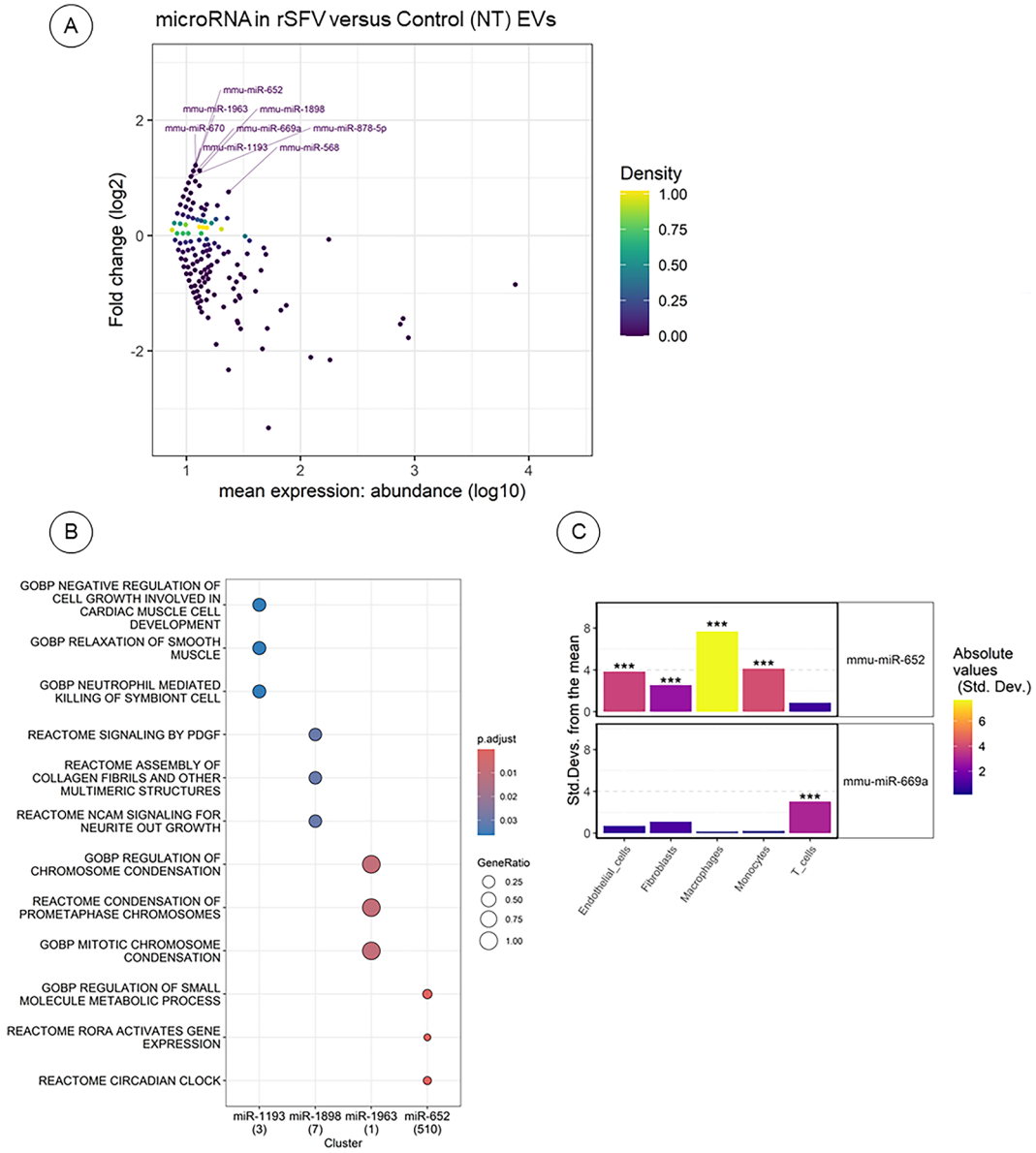

Fig. 7. Differentially Expressed Vesicular miRNAs in rSFV EVs. (**A**) Scatter plot illustrating vesicular miRNAs with elevated fold changes in EVs derived from rSFV cells. Labeled miRNAs highlight key regions based on fold change and mean expression levels (abundance). The color scale represents the density of miRNA probes overlapping the same position. (**B**) Dot plot depicting enriched pathways (adjusted $p < 0.05$) identified through hallmark (H), curated (C2), and ontology (C5) gene sets from the Molecular Signature Database (MSigDB). (**C**) Immune cell types with enriched expression of miRNA targets, based on data from the Immunologic Genome Project (ImmGen). *** indicates adjusted $p < 0.001$.

or predictive markers to screen patients that may optimally benefit from oncolytic virotherapy[21,46]. Therefore, future studies should investigate in more depth the miRNAs and other specific factors transferred by EVs and their contribution to cancer progression and therapeutic resistance.

We observe that virus infection does not only alter the cargo of EVs but also impacts the phenotype of recipient cells. For example, EVs from rSFV-infected cells enhanced the clonogenic potential of recipient melanoma cells. We can assume that this increase might possibly result from a few melanoma clones that benefitted in survival through reprogramming mediated by EVs. Although an increased survival may hint towards the development of resistance to virotherapy, we found that the sensitivity of melanoma cells towards rSFV infection remained unaltered. This could be explained by the fact that EVs from melanoma cells, which are known to transfer pro-survival signals[21,22], may be enriched with such signals upon virus infection.

In addition, our results show that rSFV infection influenced an immunomodulatory profile of melanoma EVs. Previously, EVs from B16F10 cells have been reported to have an immunosuppressive role by inducing T cell exhaustion and reprogramming macrophages to a regulatory state[23,31,33]. In line with these findings, we also

observed melanoma EVs to bear an immunosuppressive profile, however, this was not the case for rSFV-induced EVs. It could be hypothesized that this effect is partly due to altered biogenesis and/or EV cargo in rSFV-infected cells. For example, human melanoma EVs have been reported to carry regulatory checkpoint markers like PDL-1 and CD206 which may not be enriched in EVs from infected cells[23]. Whereas upon infection, cancer cells may secrete EVs with a virus-related cargo, such as single- or double-stranded RNAs and viral proteins, which in turn can activate innate pathogen recognition receptors in immune cells[3,47]. Investigating the specific factors transferred by EVs that contribute to the immunogenic effects observed in SFV EVs would be the focus of future research as it may aid in the development of novel therapeutic strategies.

Although our study focused on the effects of virotherapy using rSFV on melanoma EVs, our findings can contribute to a broader understanding of how viral infection impacts EV composition and function in cancer. And importantly to note that the use of rSFV ensures that infected cells do not produce virus, which in this study and experimental set up allowed for the isolation and systematic characterization of vesicles without virus contamination. Our results provided important insights into the immediate effects of rSFV-mediated virotherapy on the functional profile of EVs, including their microRNA cargo. In conclusion, our study provides evidence that oncolytic virotherapy can alter the biogenesis and cargo of EVs released by cancer cells. Our findings suggest that rSFV-induced immunogenic alterations in EVs could potentially influence the tumor microenvironment and could impact the response to therapy. Therefore, we support further investigation into the role of EVs in virotherapy to fully understand the impact of these vesicles on tumor progression and therapeutic outcomes.

Materials and methods

Design and production of rSFV particles

We used Semliki forest virus (SFV) based replicons that are non-replicating RNA-based virus particles capable of a single round of infection. The viruses were produced as described earlier[48] in BHK21 cells by transfection in the presence of a helper plasmid that encodes structural proteins for virus assembly and release. The rSFV particles thus produced can encode one transgene for a specific function (*gfp* for this study). Here, GFP (green fluorescent protein) works as a fluorescent marker to measure virus infectivity.

Cell lines and culture

B16F10 cells representing murine metastatic melanoma were cultured in RPMI media (Thermo Fischer Scientific, Waltham, MA, USA) with 10% fetal bovine serum (Thermo Fischer Scientific, Waltham, MA, USA) depleted of vesicles (see below) and were routinely tested for mycoplasma.

Bone marrow cells isolated from the femur of C57BL6 mice (6–8 weeks old, male) were differentiated into naïve macrophages (M0-like) in the presence of supernatant from L929 cells containing macrophage-colony stimulating factor. Thereafter these macrophages were matured into M2-like macrophages (24 h treatment with IL4 (50 ng/ml)) or M1-like macrophages (24 h treatment with interferon-gamma (50 ng/ml) and lipopolysaccharide (2 µg/ml)) for further use. Splenocytes were isolated from C57BL6 mice (6–8 weeks old, male) and immediately used for the experiments.

Macrophages and splenocytes were cultured in RPMI media with 10% fetal bovine serum depleted of vesicles. Splenocytes were cultured in the presence of 50 µM of β-mercaptoethanol (Sigma, St. Louis, MO, USA). Of note, all experiments were carried out using serum depleted of vesicles, except in the case of passaging cells and during freeze-thaw cycles. To exclude EVs present in serum, ultra-centrifugation was carried out at 100,000 g for 16 h at 4 °C (Beckman Coulter Optima XE-90, rotor SW28, Brea, California, USA).

Isolation and physical characterization of EVs

2 million B16F10 cells per flask (175 cm^2) were plated and cells were infected after 16 h of plating with 20 million virus replicon particles (MOI 10) per flask. For EVs isolation, after 24 h post-infection, cell culture media were consecutively centrifuged at 300 g for 10 min, 2 000 g for 15 min, and 10 000 g for 30 min at 4 °C. Then, the supernatant was ultra-centrifuged at 100 000 g for 2 h (Beckman Coulter Optima XE-90, rotor SW28, Brea, California, USA). The pellet enriched in EVs was washed once with PBS, submitted to ultracentrifugation at the same conditions and subsequently resuspended in PBS and stored at (-20 °C). For particle size distribution and concentration quantification, samples were diluted in PBS and loaded into NanoSight NS300 (Malvern, Worcestershire, UK) using a syringe pump. Nanoparticle movement was captured for 60 s at 25 °C for 5 times. Recorded videos were subjected to Nanoparticle Tracking Analysis (NTA) Software which determined the size distribution and concentration of EVs. In brief, the capture settings for the experiment included the use of an sCMOS camera and a Blue488 laser. The camera level was set to 12, with a slider shutter speed of 1200 and a slider gain of 146. The recording was conducted at 25.0 frames per second (FPS) for a total of 1498 frames. The temperature during the capture was maintained at 25.0 °C, and the viscosity of the medium was measured between 0.888 and 0.889 cP. The syringe pump operated at a speed of 50, and the dilution factor was 10. For analysis, the detection threshold was set to 10, with an automatic blur size. The maximum jump distance for analysis was also set to auto, ranging from 11.3 to 12.1 pixels. For each sample, 5 runs of 60 s were performed.

Zeta potential analysis of EVs

Zeta potential of EVs was measured and analyzed by Zetasizer software v7.01 (Malvern) using EV-samples (3 to 4×10^9 EVs/ml) diluted in PBS for each group. For each sample, 10 runs of 10 s were performed at 25oC and equilibration time of 60 s.

Western blot

10^9/ml SFV and NT EVs in RIPA buffer were sonicated (3 pulses of 5 s at low amplitude) using a probe sonicator (Fisher Brand, Hampton, New Hampshire, USA). Then, samples were kept on ice for 15 min and centrifuged

at 12 000 rpm for 15 min at 4ºC. Next, the supernatant was transferred to new tubes and diluted (1:1) with a denaturing loading buffer and samples were boiled for 5 min at 100ºC. Then, samples were loaded onto 10% SDS-PAGE (0.375 M Tris, pH 8.8, 0.1% SDS, 10% acrylamide, 0.03% ammonium persulfate, and 0.06% N, N, N′, N′-tetramethyl ethylenediamine). After electrophoresis, the separated proteins were transferred onto the PVDF membrane (GE Healthcare, Chicago, Illinois, USA) and the membrane was blocked with 5% BSA in 0.1% TBS-Tween for 1 h at room temperature. Next, immunoblotting was performed with anti-CD63 (1:700, Thermo Fisher Scientific, Waltham, MA, USA) and anti-CD9 (1:500, Thermo Fisher Scientific, Waltham, MA, USA) overnight at 4ºC and secondary antibody incubation (1:7000, anti-rabbit IgG Peroxidase, Sigma, St. Louis, MO, USA) for 1 h at room temperature. Protein bands were detected with a chemiluminescent kit (GE Healthcare, Chicago, Illinois, USA).

Transmission electron microscopy of EV isolates

50 µl of isolated EVs in PBS were spotted on a copper grid and staining was performed using PTK (Post-Embedding Tissue Kit) as manufacturer's instructions. Images were acquired using the Jeol JEM 1011 Transmission Electron Microscope and presented in the figures without any further processing. The size of observed particles was measured with reference to the scale present in the image. Negative control samples were performed using filtered PBS.

Staining and EVs uptake assay

EVs were stained with PKH26 dye (Sigma-Aldrich) following the manufacturer's instructions. Briefly, 2 µL of PKH26 dye was diluted in 500 µL of Diluent C and then combined with 500 µL of EVs at a 1:1 ratio. The mixture was incubated at room temperature for 5 min. To remove excess dye, the mixture was filtered using MW3000 columns (Invitrogen-Thermo Fisher Scientific). B16F10 cells were incubated overnight with 10^8 EVs/ml concentrations of stained EVs. After incubation, the cells were washed with PBS to eliminate any non-incorporated EVs. Images were collected via EVOS microscopy platform (Thermo Fisher Scientific, Waltham, MA, USA). Uptake of vesicles by individual cells was analyzed using Cell Profiler software (http://www.cellprofiler.org) by manually labeling individual cells and quantifying the number of (PKH26+) fluorescent spots per cell. EV uptake kinetics was assessed using flow cytometry at 1,2,4, and 6 h post incubation of B16F10 cells with PKH26-stained EVs.

In vivo tumor engraftment

B16F10 cells were treated in vitro with vesicles (10^7 EVs/ml) every day for 5 days and then later collected for subcutaneous tumor engraftment in C57BL6 mice (male, 7 weeks old) in the ventral region of each animal. Mice were s.c. injected with 0.2 million cells resuspended in RPMI media and animals were monitored daily. Tumor growth in time was monitored by performing tumor measurements using a digital caliper. Animals with a measurable tumor (> 100 mm^3) were considered to have a successful engraftment, followed by a Kaplan-Meier analysis to determine changes in the probability of tumor engraftment in time due to the pretreatment by EVs from infected cells. Tumor growth rate was assessed by starting the measurement when tumors become measurable (> 100 mm^3) and continuing until the tumors reach or exceed a size of 1 cubic centimeter. Animals were kept under a 12:12 light-dark cycle with food and water ad libitum. In vivo experiments were conducted according to legislation for animal research in Brazil with approval from the Committee on Ethics of Animal Experiments of the University of São Paulo (# 1808/2022).

Clonogenic assay

B16F10 cells were treated with vesicles (10^7 EVs/ml) every day for 5 days and/or treated with rSFV particles (MOI-10) at day 4 in the presence of EVs (Supplementary Fig. 3). After treatment, 200 cells were plated in a 6-well plate and when colonies in the control group reached around 30 to 50 cells (7 days), the cells were washed with PBS and fixed with PBS/formaldehyde 4% for 15 min. Cells were washed again with PBS and incubated with crystal violet 0.1% for 10 min. After three washes with PBS, the plate was left to dry and then colonies were counted. The assay was performed according to the instructions provided by Franken and colleagues[49].

Resistance to viral infection assay

6×10^3 B16F10 cells were treated daily for 3 days with different concentrations of EVs (10^8-10^9 EVs/ml) from infected or uninfected cells. Then 15×10^3 of these pre-treated B16F10 cells were re-plated per well in a 96-well plate in the presence of EVs. Upon reaching a confluence of 70%, these cells were infected with rSFV-GFP (MOI-10), again in the presence of fresh EVs (10^8-10^9 EVs/ml). 24 h after infection, cells were detached and resuspended in PBS for analysis of GFP + cells by flow cytometry (Attune, Thermo Fischer Scientific, Waltham, MA, USA).

Tumor-immune co-culture assay

Freshly isolated splenocytes from healthy C57BL/6 mice (male, 7–8 weeks old) were co-cultured for 48 h with B16F10 cells pre-treated with EVs. Briefly, B16F10 cells were treated with 10^8 EVs/ml every day for 5 days. After treatment, B16F10 cells were re-plated with freshly isolated splenocytes in a 1:5 tumor cells: splenocyte ratio. After 48 h of co-culture, cells were detached and processed for flow cytometry. Tumor cells (higher sideward and forward scatter) and lymphocytes (lower sideward and forward scatter) were identified based on their size and complexity. Dead tumor cells were identified by their loss of cellular volume and size (lower forward scatter). Apoptotic cells were observed by staining for caspase 3 and 7 activity (CellEvent™ Caspase3/7 Green detection reagent, Invitrogen) as per the recommended protocol. Antibodies optimized for flow cytometry were used to

identify helper T cells (PE, anti-mouse CD4, Biolegend), cytotoxic T cells (APC, anti-mouse CD8, Biolegend) and activated T cells (PE-Cy-7, anti-mouse CD69, Biolegend) through surface staining.

Macrophage phenotype assay

Bone marrow-derived cells were collected from C57BL/6 mice femur (male, 7–8 weeks old) and cultivated with RPMI media containing 30% L929-conditioned media and 15% FBS for 6 days. Then, one million cells were incubated with Fc block (1 µg) for 1 h at 4ºC. Next, anti-F4/80-PE (0.25 µg; BD Biosciences, Franklin Lakes, New Jersey, USA) or isotype control (0.25 µg; anti-rat-IgG2a, Thermo Fischer Scientific, Waltham, MA, USA) was added to samples for 45 min at 4ºC and immunostaining of F4/80 positive cells, representing macrophages, were quantified by flow cytometry (Attune, Thermo Fischer Scientific, Waltham, MA, USA). To address the role of EVs on macrophage polarization, F4/80^{+} macrophages were plated (4 million cells per plate) in RPMI supplemented with 10% FBS for M0, LPS (1 µg/mL; Sigma) and IFN-γ (50 ng/mL) for M1 or IL-4 (50 ng/mL; R&D Systems, Minneapolis, Minnesota, USA) for M2 during 24 hs. Then, M0-like, M1-like or M2-like macrophages were treated with EVs (10^8 EVs/ml) from infected or uninfected cells for 24 h. After treatment, cells were detached and processed for RNA extraction using TRIzol according to manufacturer's instructions (Thermo Fischer Scientific, Waltham, MA, USA). cDNA was synthesized using 2 µg of isolated RNA using the High capacity kit (Thermo Fischer Scientific, Waltham, MA, USA), and Real-Time PCR was performed using SYBR Green I chemistry (Thermo Fischer Scientific, Waltham, MA, USA). Primers used for murine markers are as follows: *Il12* (Forward: 5′-AGCAGTAGCAGTTCCCCTGA-3′; Reverse: 5′-AGTCCCTTTGGTCCAGTGTG-3′), *iNOS* (Forward 5′-CAGGAACCTACCAGCTCACTCT-3′; Reverse 5′-ATGTGCTGAAACATTTCCTGTG-3′), *Mrc1* (Forward 5′-TTTGCAAGCTTGTAGGAAGGA-3′; Reverse 5′-CCAATCCACAGCTCATCATTT-3′), *Arg-1* (Forward 5′-GAACCCAACTCTTGGGAAGAC-3′; Reverse 5′-GGAGAAGGCGTTTGCTTAGTT-3′) and *Il10* (Forward 5′-ACTTGCTCTTGCACTACCAAAGCC-3′; Reverse 5′-GCATGTGGCTCTGGCCGACTG-3′) and *Hprt* as endogenous control (Forward 5′-AGGCCAGACTTTGTTGGATTT-3′; Reverse 5′-GGCTTTGTATTTGGCTTTTCC-3′). The relative gene expression (fold change) was obtained using the delta-delta Ct method, according to Livak and Schmittgen, and cells treated with EVs from uninfected cells were used as reference sample[50].

Splenocyte proliferation assay

10 to 15 million freshly isolated splenocytes were labeled with CFSE (2.5 µM; Thermo Fisher Scientific, Waltham, MA, USA) for 10 min and then stimulated with a combination of phorbol myristate acetate (PMA, 10 µg/ml; Sigma, St. Louis, MO, USA) and ionomycin (250 ng/ml; Sigma, St. Louis, MO, USA) in RPMI media with 10% FBS and (50 µM) β-mercaptoethanol (Sigma, St. Louis, MO, USA). Thereafter, 0.2 million splenocytes per condition per well were allowed to proliferate for 48 h in the presence of different EVs (10^8/ml). After treatment, cells were resuspended in PBS and processed for flow cytometry (Attune, Thermo Fisher Scientific, Waltham, MA, USA) to observe proliferation profile based on CFSE. The protocol was performed as per the instructions provided by Quah and colleagues[51].

Quantification of microRNAs from in vitro EV-preparations

EVs from infected or non-infected B16F10 cells in vitro were processed for miRNA extraction using the miRNeasy Tissue/Cells Advanced Mini Kit (Qiagen, Hilden, Germany). Vesicular miRNA (EV-miRNA) content was determined using the MOUSE V1.5 MIRNA ASSAY CSO (Nanostring Technologies, Seattle, Washington, USA) through hybridization with specific probes attached to barcodes on their corresponding miRNA targets. After detecting and acquiring images for individual counting of miRNAs, data were analyzed using the nSolver software v.3.0. The geometric mean from negative control probes was used as a threshold to avoid false positives. Data were then normalized using the most stable miRNAs between groups (up to 25% coefficient of variation) as endogenous controls, to determine the most abundant miRNAs expressed in each group.

Cell type enrichment test and gene set enrichment analysis (GSEA)

We utilized the multiMiR database (http://multimir.org/) via the R package 'multiMiR' to identify all validated murine targets for miRNAs relevantly overexpressed in the rSFV group. These gene lists were subsequently employed to perform an immune cell type enrichment analysis, using expression data from the Immunologic Genome Project (ImmGen)[52]. Additionally, we conducted Gene Set Enrichment Analysis (GSEA) using gene sets from the Molecular Signatures Database (https://www.gsea-msigdb.org/gsea/msigdb/), including categories H (hallmark gene sets), C2 (curated gene sets), and C5 (ontology gene sets)[53]. Enrichment results were considered significant based on adjusted p-values < 0.05.

Statistical analysis

One-way ANOVA was used to calculate significance. Statistical differences were considered when $p \leq 0.05$ and Bonferroni's correction was applied for multiple comparisons. For microRNA analysis, Benjamini-Hochberg was performed.

Data availability

Normalized Data from barcoding Nanostring are provided as a Supplementary Table. All methods were carried out in accordance with relevant guidelines and regulations.

Received: 11 December 2023; Accepted: 4 December 2024
Published online: 04 January 2025

References

1. Cocozza, F., Grisard, E., Martin-Jaular, L., Mathieu, M. & Théry, C. SnapShot: extracellular vesicles. *Cell* **182**, 262–262e1. https://doi.org/10.1016/j.cell.2020.04.054 (2020).
2. Colombo, M., Raposo, G. & Théry, C. Biogenesis, secretion, and intercellular interactions of exosomes and other extracellular vesicles. *Annu. Rev. Cell Dev. Biol.* **30**, 255–289. https://doi.org/10.1146/annurev-cellbio-101512-122326 (2014).
3. Pegtel, D. M. & Gould, S. J. *Exosomes Annu. Rev. Biochem.* **88**, 487–514. https://doi.org/10.1146/annurev-biochem-013118-111902. (2019).
4. Schorey, J. S., Cheng, Y., Singh, P. P. & Smith, V. L. Exosomes and other extracellular vesicles in host-pathogen interactions. *EMBO Rep.* **16**, 24–43. https://doi.org/10.15252/embr.201439363 (2015).
5. Alenquer, M. & Amorim, M. Exosome biogenesis, regulation, and function in viral infection. *Viruses* **7**, 5066–5083. https://doi.org/10.3390/v7092862 (2015).
6. Dogrammatzis, C., Waisner, H. & Kalamvoki, M. Cloaked viruses and viral factors in cutting edge exosome-based therapies. *Front. Cell. Dev. Biol.* **8**, 376. https://doi.org/10.3389/fcell.2020.00376 (2020).
7. Lv, P. et al. Genetically engineered cell membrane nanovesicles for oncolytic adenovirus delivery: a versatile platform for cancer virotherapy. *Nano Lett.* **19**, 2993–3001. https://doi.org/10.1021/acs.nanolett.9b00145 (2019).
8. Ruiz-Guillen, M. et al. Capsid-deficient alphaviruses generate propagative infectious microvesicles at the plasma membrane. *Cell. Mol. Life Sci.* **73**, 3897–3916. https://doi.org/10.1007/s00018-016-2230-1 (2016).
9. Saari, H. et al. Extracellular vesicles provide a capsid-free vector for oncolytic adenoviral DNA delivery. *J. Extracell. Vesicles*. **9**, 1747206. https://doi.org/10.1080/20013078.2020.1747206 (2020).
10. Zhou, C. et al. Exosomes carry microRNAs into neighboring cells to promote diffusive infection of newcastle disease virus. *Viruses* **11**, E527. https://doi.org/10.3390/v11060527 (2019).
11. Labani-Motlagh, A., Naseri, S., Wenthe, J., Eriksson, E. & Loskog, A. Systemic immunity upon local oncolytic virotherapy armed with immunostimulatory genes may be supported by tumor-derived exosomes. *Mol. Ther. Oncolytics*. **20**, 508–518. https://doi.org/10.1016/j.omto.2021.02.007 (2021).
12. Wedge, M. E. et al. Virally programmed extracellular vesicles sensitize cancer cells to oncolytic virus and small molecule therapy. *Nat. Commun.* **13**, 1898. https://doi.org/10.1038/s41467-022-29526-8 (2022).
13. Nolte-'t Hoen, E., Cremer, T., Gallo, R. C. & Margolis, L. B. Extracellular vesicles and viruses: Are they close relatives? *Proc. Natl. Acad. Sci. USA. 113*, 9155–9161 https://doi.org/10.1073/pnas.1605146113 (2016).
14. Zhou, Y., McNamara, R. P. & Dittmer, D. P. Purification methods and the presence of RNA in virus particles and extracellular vesicles. *Viruses* **12**, 917. https://doi.org/10.3390/v12090917 (2020).
15. Kakiuchi, Y. et al. Local oncolytic adenovirotherapy produces an abscopal effect via tumor-derived extracellular vesicles. *Mol. Ther.* **29**, 2920–2930. https://doi.org/10.1016/j.ymthe.2021.05.015 (2021).
16. Smerdou, C. & Liljeström, P. Two-helper RNA system for production of recombinant Semliki forest virus particles. *J. Virol.* **73**, 1092–1098. https://doi.org/10.1128/JVI.73.2.1092-1098.1999 (1999).
17. Liljeström, P. & Garoff, H. A new generation of animal cell expression vectors based on the Semliki Forest virus replicon. *Biotechnol. (N Y)*. **9**, 1356–1361 (1991).
18. Singh, A., Koutsoumpli, G., van de Wall, S. & Daemen, T. An alphavirus-based therapeutic cancer vaccine: from design to clinical trial. *Cancer Immunol. Immunother*. **68**, 849–859. https://doi.org/10.1007/s00262-018-2276-z (2019).
19. Komdeur, F. L. et al. First-in-human phase I clinical trial of an SFV-based RNA replicon cancer vaccine against HPV-induced cancers. *Mol. Ther.* **29** (2), 611–625. https://doi.org/10.1016/j.ymthe.2020.11.002 (2021).
20. Zhou, Q. et al. Tumor-derived extracellular vesicles in melanoma immune response and immunotherapy. *Biomed. Pharmacother*. **156**, 113790. https://doi.org/10.1016/j.biopha.2022.113790 (2022).
21. Santos, N. L., Bustos, S. O., Bhatt, D., Chammas, R. & Andrade, L. N. D. S. Tumor-derived extracellular vesicles: modulation of cellular functional dynamics in tumor microenvironment and its clinical implications. *Front. Cell. Dev. Biol.* **9**, 737449. https://doi.org/10.3389/fcell.2021.737449 (2021).
22. Andrade, L. N. et al. Extracellular vesicles shedding promotes melanoma growth in response to chemotherapy. *Sci. Rep.* **9** https://doi.org/10.1038/s41598-019-50848-z (2019).
23. Chen, G. et al. Exosomal PD-L1 contributes to immunosuppression and is associated with anti-PD-1 response. *Nature* **560**, 382–386. https://doi.org/10.1038/s41586-018-0392-8 (2018).
24. Poggio, M. et al. Suppression of exosomal PD-L1 induces systemic anti-tumor immunity and memory. *Cell* **177**, 414–427e13. https://doi.org/10.1016/j.cell.2019.02.016 (2019).
25. Chen, J. et al. Tumor extracellular vesicles mediate anti-PD-L1 therapy resistance by decoying anti-PD-L1. *Cell. Mol. Immunol.* **19**, 1290–1301. https://doi.org/10.1038/s41423-022-00926-6 (2022).
26. Tominaga, N. et al. RPN2-mediated glycosylation of tetraspanin CD63 regulates breast cancer cell malignancy. *Mol. Cancer*. **13**, 134. https://doi.org/10.1186/1476-4598-13-134 (2014).
27. Cheng, Y. C. et al. The roles of extracellular vesicles in malignant melanoma. *Cells* **10**, 2740. https://doi.org/10.3390/cells10102740 (2021).
28. Hood, J. L. Natural melanoma-derived extracellular vesicles. *Semin Cancer Biol.* **59**, 251–265. https://doi.org/10.1016/j.semcancer.2019.06.020 (2019).
29. Matsumoto, A. et al. Accelerated growth of B16BL6 tumor in mice through efficient uptake of their own exosomes by B16BL6 cells. *Cancer Sci.* **108**, 1803–1810. https://doi.org/10.1111/cas.13310 (2017).
30. Yin, Y. et al. Colorectal cancer-derived small extracellular vesicles promote tumor immune evasion by upregulating PD-L1 expression in tumor-associated macrophages. *Adv. Sci.* **9**, 2102620. https://doi.org/10.1002/advs.202102620 (2022).
31. Bardi, G. T., Smith, M. A. & Hood, J. L. Melanoma exosomes promote mixed M1 and M2 macrophage polarization. *Cytokine* **105**, 63–72. https://doi.org/10.1016/j.cyto.2018.02.002 (2018).
32. Morrissey, S. M. et al. Tumor-derived exosomes drive immunosuppressive macrophages in a pre-metastatic niche through glycolytic dominant metabolic reprogramming. *Cell. Metab.* **33**, 2040–2058e. https://doi.org/10.1016/j.cmet.2021.09.002 (2021).
33. Gupta, P. et al. Tumor derived extracellular vesicles drive t cell exhaustion in tumor microenvironment through sphingosine mediated signaling and impacting immunotherapy outcomes in ovarian cancer. *Adv. Sci.* **9**, e2104452. https://doi.org/10.1002/advs.202104452 (2022).
34. Thakur, A. et al. Label-free sensing of exosomal MCT1 and CD147 for tracking metabolic reprogramming and malignant progression in glioma. *Sci. Adv.* **6**, eaaz6119. https://doi.org/10.1126/sciadv.aaz6119 (2020).
35. Bardi, G. T., Al-Rayan, N., Richie, J. L., Yaddanapudi, K. & Hood, J. L. Detection of inflammation-related melanoma small extracellular vesicle (sEV) mRNA content using primary melanocyte sEVs as a reference. *Int. J. Mol. Sci.* **20**, 1235. https://doi.org/10.3390/ijms20051235 (2019).
36. Liu, Y., Li, M., Liu, H., Kang, C. & Wang, C. Cancer diagnosis using label-free SERS-based exosome analysis. *Theranostics* **14**, 1966–1981 https://doi.org/10.7150/thno.92621 (2024).
37. Mathieu, M. et al. Specificities of exosome versus small ectosome secretion revealed by live intracellular tracking of CD63 and CD9. *Nat. Commun.* **12**, 4389. https://doi.org/10.1038/s41467-021-24384-2 (2021).
38. Earnest, J. T. et al. The tetraspanin CD9 facilitates MERS-coronavirus entry by scaffolding host cell receptors and proteases. *PLoS Pathog.* **13**, e1006546. https://doi.org/10.1371/journal.ppat.1006546 (2017).

39. York, S. B. et al. Zika virus hijacks extracellular vesicle tetraspanin pathways for cell-to-cell transmission. *mSphere* **6**, e0019221 https://doi.org/10.1128/mSphere.00192 (2021).
40. Ninomiya, M. et al. The exosome-associated tetraspanin CD63 contributes to the efficient assembly and infectivity of the hepatitis B virus. *Hepatol. Commun.* **5**, 1238–1251. https://doi.org/10.1002/hep4.1709 (2021).
41. Stiles, K. M. & Kielian, M. Role of TSPAN9 in alphavirus entry and early endosomes. *J. Virol.* **90**, 4289–4297. https://doi.org/10.1128/JVI.00018-16 (2016).
42. Hirigoyen, U. et al. Oncolytic viruses alter the biogenesis of tumor extracellular vesicles and influence their immunogenicity. *Mol. Ther. Oncol.* https://doi.org/10.1016/j.omton.2024.200887 (2024).
43. Sun, Z. et al. Effect of exosomal miRNA on cancer biology and clinical applications. *Mol. Cancer*. **17** https://doi.org/10.1186/s12943-018-0897-7 (2018).
44. Robbins, P. D. & Morelli, A. E. Regulation of immune responses by extracellular vesicles. *Nat. Rev. Immunol.* **14**, 195–208. https://doi.org/10.1038/nri3622 (2014).
45. Xia, T. et al. Advances in the role of STAT3 in macrophage polarization. *Front. Immunol.* **14**, 1160719. https://doi.org/10.3389/fimmu.2023 (2023).
46. Mumford, S. L. et al. Circulating microRNA biomarkers in melanoma: tools and challenges in personalised medicine. *Biomolecules* **8**, 21. https://doi.org/10.3390/biom8020021 (2018).
47. Kouwaki, T., Okamoto, M., Tsukamoto, H., Fukushima, Y. & Oshiumi, H. Extracellular vesicles deliver host and virus RNA and regulate innate immune response. *Int. J. Mol. Sci.* **18**, 666. https://doi.org/10.3390/ijms18030666 (2017).
48. Daemen, T., Regts, J., Holtrop, M. & Wilschut, J. Immunization strategy against cervical cancer involving an alphavirus vector expressing high levels of a stable fusion protein of human papillomavirus 16 E6 and E7. *Gene Ther.* **9**, 85–94. https://doi.org/10.1038/sj.gt.3301627 (2002).
49. Franken, N. A. P., Rodermond, H. M., Stap, J., Haveman, J. & van Bree, C. Clonogenic assay of cells in vitro. *Nat. Protoc.* **1**, 2315–2319. https://doi.org/10.1038/nprot.2006.339 (2006).
50. Livak, K. J. & Schmittgen, T. D. Analysis of relative gene expression data using real-time quantitative PCR and the 2(-Delta Delta C(T)) method. *Methods* **25**, 402–408. https://doi.org/10.1006/meth.2001.1262 (2001).
51. Quah, B. J. C., Warren, H. S. & Parish, C. R. Monitoring lymphocyte proliferation in vitro and in vivo with the intracellular fluorescent dye carboxyfluorescein diacetate succinimidyl ester. *Nat. Protoc.* **2**, 2049–2056. https://doi.org/10.1038/nprot.2007.296 (2007).
52. Immunological Genome Project. ImmGen at 15. *Nat. Immunol.* **21** (7), 700–703. https://doi.org/10.1038/s41590-020-0687-4 (2020).
53. Subramanian, A. et al. Gene set enrichment analysis: a knowledge-based approach for interpreting genome-wide expression profiles. *Proc. Natl. Acad. Sci. USA* **102** (43), 15545–15550. https://doi.org/10.1073/pnas.0506580102 (2005).

Acknowledgements

We acknowledge all members of the technical support from our institute, CTO-ICESP, Prof. Dr. Ana Paula Lepique (ICB-IV, USP) for the guidance in the flow cytometry analysis, and the technical assistance provided by Márcio de Carvalho from Nanostring Core (Experimental Research Unity, UNESP). We also would like to thank the Electron Microscopy Center of the Adolfo Lutz Institute for the images obtained using the Jeol JEM 1011 Transmission Electron Microscope and for the technical support.

Author contributions

DB was responsible for the experiments, conceptualization, formal analysis, interpreting results, plotted data and writing-original draft; AB was responsible for SFV replicon particles construction and production; SOB performed WB and EVs characterization; AHO performed the in vivo experiments; AGMC conducted the microRNA analysis; PPR was responsible for microRNA data acquisition; RC, TD and LNSA were responsible for conceptualization, supervision, writing–review and editing. All authors approved the final version and agreed to submit the manuscript.

Funding

This research was supported by grants from FAPESP (Fundação de Amparo à Pesquisa do Estado de São Paulo, grant Number 2020/09176-8), CAPES (Coordenação de Aperfeiçoamento de Pessoal de Nível Superior, Finance Code 001) PhD scholarship for DB, and GSMS-ATTP (University of Groningen, Graduate school of Medical Sciences, Abel Tasman Talent program) PhD scholarship for DB.

Declarations

Competing interests

The authors declare no competing interests.

Additional information

Supplementary Information The online version contains supplementary material available at https://doi.org/10.1038/s41598-024-82331-9.

Correspondence and requests for materials should be addressed to R.C. or L.N.d.S.A.